nature physics

Article

https://doi.org/10.1038/s41567-022-01767-w

Ultrafast visualization of an electric field under the Lorentz transformation

In the format provided by the authors and unedited

Supplementary information:

Ultrafast visualization of an electric field under the Lorentz transformation

Masato Ota[1], Koichi Kan[2*], Soichiro Komada[3], Youwei Wang[1,4], Verdad C. Agulto[1], Valynn Katrine Mag-usara[1], Yasunobu Arikawa[1], Makoto R. Asakawa[4], Youichi Sakawa[1], Tatsunosuke Matsui[3], and Makoto Nakajima[1*]

[1]Institute of Laser Engineering, Osaka University
[2]Institute of Scientific and Industrial Research (SANKEN), Osaka University
[3]Department of Electrical and Electronic Engineering, Mie University
[4]Faculty of Engineering Science, Kansai University

E-mail: nakajima.makoto.ile@ile.osaka-u.ac.jp

Contents

1. Theoretical calculations of the electric field around a negative point charge under the Lorentz transformation

A static negative point charge in an inertial system K' generates an isotropic electric field, as shown in Supplementary Fig. 1a; the electric field is written as $\boldsymbol{E}'(\boldsymbol{r}',t') = \frac{q}{4\pi\varepsilon_0 r'^2}\frac{\boldsymbol{r}'}{r'}$, where q is the charge amount, ε_0 is the vacuum permittivity, and $r' = |\boldsymbol{r}'|$. When a negative point charge constantly moves with a high velocity, the electric field contracts in the propagation direction of the beam and extends in the radial direction, as shown in Supplementary Fig. 1b; the electric field observed in an inertial system K moving with a relative velocity $c\boldsymbol{\beta}$ regarding the inertial system K' is expressed as

$$\boldsymbol{E}_{SR}(\boldsymbol{R},t) = \frac{1}{4\pi\varepsilon_0 R^2}\frac{\boldsymbol{R}}{R}\frac{1}{(1-\beta^2)^{1/2}}\frac{1}{\left(1+\frac{\beta^2}{1-\beta^2}\cos^2\theta\right)^{3/2}}, \tag{1}$$

where $\boldsymbol{R} = \boldsymbol{r} - c\boldsymbol{\beta}t$ and $\cos\theta = \frac{\boldsymbol{R}}{R}\cdot\frac{\boldsymbol{\beta}}{\beta}$. On the surfaces of constant electric field strengths $|\boldsymbol{E}_{SR}(\boldsymbol{R},t)| = \text{const}$, the relation of $\frac{\{x^2+y^2+\gamma^2(z-c\beta t)^2\}^3}{x^2+y^2+(z-c\beta t)^2} = \text{const}$ is satisfied, where $\gamma = 1/\sqrt{1-\beta^2}$ and the propagation direction of the charge is assumed to be along the z-axis for simplicity.

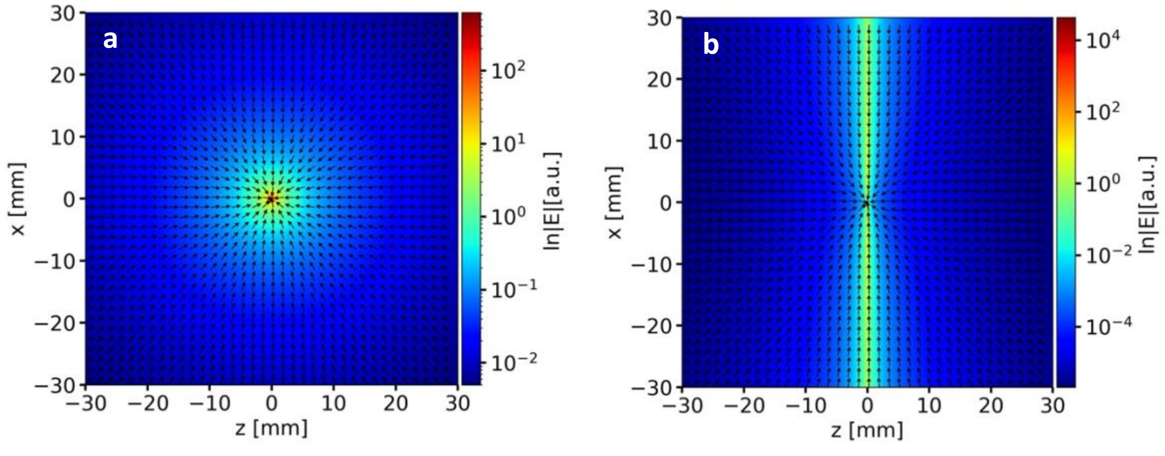

Supplementary Fig. 1 | Theoretical calculations of the electric field around a negative point charge under the Lorentz transformation. a, **b**, 2D electric field profiles around a negatively charged particle with energies of 0 and 35 MeV, respectively. Here, the absolute electric field strength is shown by the color bar and the direction is denoted by the black vectors.

2. Convolution between the Gaussian profile and the electric field profile around a relativistic point charge

To describe the electric field around a bunch of charged particles $\boldsymbol{E}_{\text{bunch}}(\boldsymbol{r},t)$, we need to convolute a 3D density profile of an electron bunch with a 3D electric field around a point charge: $\boldsymbol{E}_{\text{bunch}}(\boldsymbol{r},t) = \rho(\boldsymbol{r},t) * \boldsymbol{E}_{\text{point}}(\boldsymbol{r},t)$, where $\rho(\boldsymbol{r},t)$ is the density profile of the bunch and $\boldsymbol{E}_{SR}(\boldsymbol{R},t)$ in Eq. (1) can be inserted into $\boldsymbol{E}_{\text{point}}(\boldsymbol{r},t)$. The $\rho(\boldsymbol{r},t)$ and $E_{x,\text{point}}(\boldsymbol{R},t)$ are shown in Supplementary Figs. 2a, b, respectively. Here, we assume that the beam profile is a Gaussian in the longitudinal and transverse directions:

$$\rho(\boldsymbol{r},t) = \rho(x,y,z,t) = \rho_0 \exp\left[-\frac{x^2+y^2}{2{\sigma_t}^2} - \frac{(z-c\beta t)^2}{2{\sigma_l}^2}\right], \tag{2}$$

where the x- and y-axes are on the transverse plane, the z-axis is the longitudinal (propagation) direction, ρ_0 is the constant charge density, and σ_{t} and σ_{l} correspond to the transverse diameter and the longitudinal pulse width in root mean square (RMS) of the electron bunch, respectively. The transverse electric field E_x ($\boldsymbol{E}_{\text{bunch}}(\boldsymbol{r},t)$ in the x-direction) in the xz-plane ($y=0$) around an electron beam of which the beam sizes correspond to the experimental measurement (the transverse and longitudinal sizes were 3.5 mm and 0.72 ps, respectively, as discussed later)

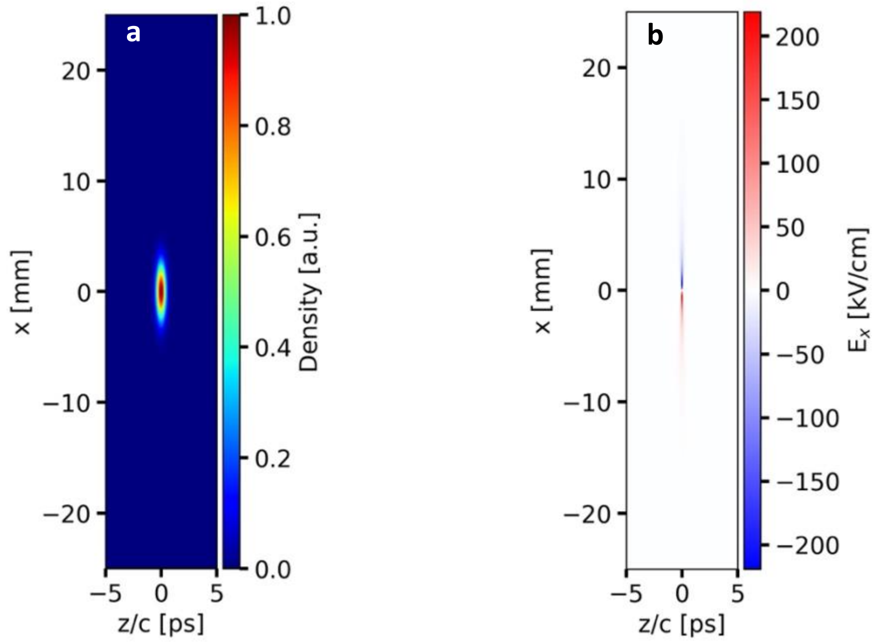

Supplementary Fig. 2 | Numerical convolution between the Gaussian profile and the electric field profile around a relativistic point charge. a, A 2D density profile of a Gaussian beam in the xz-plane ($\rho(\boldsymbol{r},t)$ at $y=0$) defined by Eq. (2). Here, we used the experimentally obtained beam sizes: beam diameter of 3.5 mm and pulse width of 0.72 ps (FWHM). **b**, A 2D electric field profile ($\boldsymbol{E}_{\text{point}}(\boldsymbol{R},t)$ in the x-direction at $y=0$) around a point charge (infinitesimal electron beam) constantly moving in the z-axis positive direction with an energy of 35 MeV. Here, the calculation box (discrete space: $550\times550\times120$) is set relatively larger than its counterpart in Fig. 2b because the boundary of the box can cause an error in the convolution. Therefore, we cropped the convoluted image and show the central part in Fig. 2b.

is visualized in Fig. 2b by conducting the numerical convolution, where the integration regions are the whole areas of Supplementary Figs. 2a,b. Because the LT does not consider the metallic boundary, we use the relative position Z in the horizontal axis instead of the absolute coordinate z in Fig. 2b.

3. Properties of the electron beam generated by the linear accelerator

In this section, we discuss the properties of the electron beam: the charge amount, the transverse beam size, and the timing jitter between the electron beam and the probe pulse. The charge amount and the transverse beam size are used as a basis for the analysis of whole experimental results, i.e., Fig. 2a and Figs. 3a–d. The timing jitter is shown as error bars in Figs. 3e–h.

The electron bunches were generated by a photocathode linac at the Institute of Scientific and Industrial Research (SANKEN), Osaka University. The electron linac comprised a photocathode radio-frequency gun, a linac, and a magnetic bunch compressor[48]. Electron bunches were generated by femtosecond ultraviolet pulses with a central wavelength of 266 nm and a pulse energy of 80 μJ/pulse from a third-harmonic generation of a Ti:sapphire femtosecond laser with a regenerative amplifier. The electron beams with an energy of 35 MeV passed through the exit of the accelerator tube (Ti window), and the electric field was measured by EO sampling in the air.

The charge amount of the electron bunch was acquired through a current transformer located immediately after the Ti window and was estimated from a measurement of the induced current inside the coils.

The transverse beam size was measured by injecting the electron beam onto a Gd_2O_2S:Tb-based scintillator (Mitsubishi Chemical: DRZ-High) and taking a photograph of the fluorescence (Supplementary Figs. 3a, b). We note that the obtained spatial profile was temporally integrated.

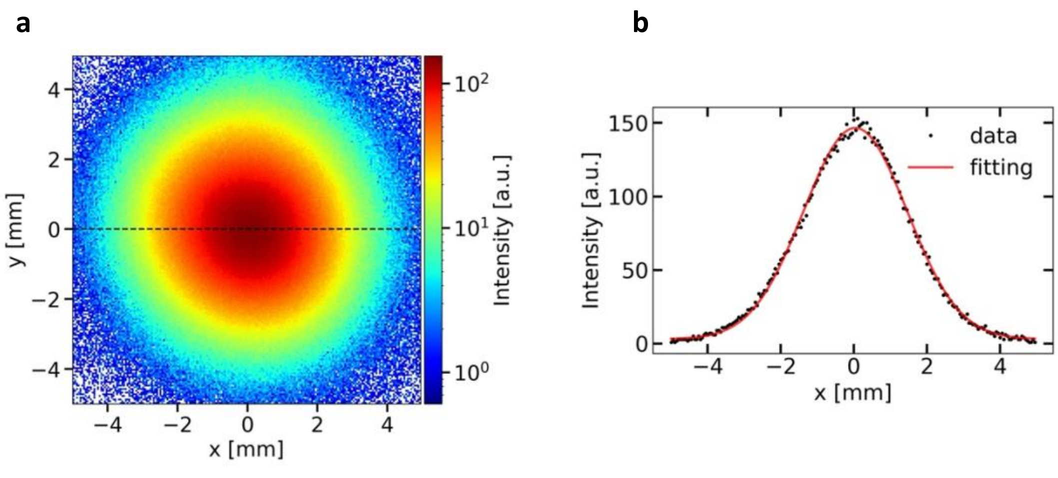

Supplementary Fig. 3 | Transverse beam size. a, An image of the fluorescence generated by injecting a relativistic electron bunch into a scintillator. This fluorescence is proportional to the density profile of the electron bunch. The transverse electron beam profile shows axial symmetry around the z-axis. **b**, A horizontal lineout of the electron density profile obtained across the black dashed line in **a**. Black circles are the data points; this profile is fitted with a Gaussian function (red curve), and the beam size (diameter) is estimated as 3.5 mm (FWHM).

The jitter of the arrival time on the ZnTe between the electron beam and the probe laser was monitored by spatial decoding[49]. The probe pulse with a spot size of 2.5 mm × 5 mm was injected into the ZnTe crystal with an incidence angle $\psi = 45°$, whereas the electron beam passed through the crystal perpendicular to the surface. In this geometry, the arrival time of the probe laser on the crystal surface differed with regard to its spatial profile. We used the crossed-Nicol configuration to extract the probe signal whose polarity was modulated by the Pockels effect. In this configuration, two polarizers with a relative angle of 90° were located upstream and downstream of the EO crystal. Therefore, the temporal evolution of the THz electric field pulse was measured by a CCD camera in a single shot. Notably, this measurement could not obtain a pure spatiotemporal profile of the electric field because the temporal evolution was given at each different position on the crystal. To obtain the pure spatiotemporal profile, the temporal electric field profile along a narrow line on the EO crystal surface must be investigated[50,51]. Moreover, using a line on the surface of the EO crystal instead of the whole area suppresses the effect of the nonuniform EO constant inside the crystal. However, the spatial decoding method is useful to obtain the arrival timing of the electron beam because of its simplicity. Supplementary Fig. 4a shows one of the images of the spatial decoding. Here, the horizontal axis dT $(= x\cos\psi/c)$ and the vertical axis y correspond to time and space, respectively. The vertical yellow line is the signal of the electric field. The red curve is a lineout obtained by averaging the temporal evolution on the y-axis. Consecutively obtained timing jitter (i.e., shot-by-shot relative arrival timing of the electron beam) is shown in Supplementary Fig. 4b. Here, the maximum peak in the temporal evolution was chosen as the arrival time; the obtained timing jitter was 0.43 ps (RMS), and the interval between shots was ~10 s.

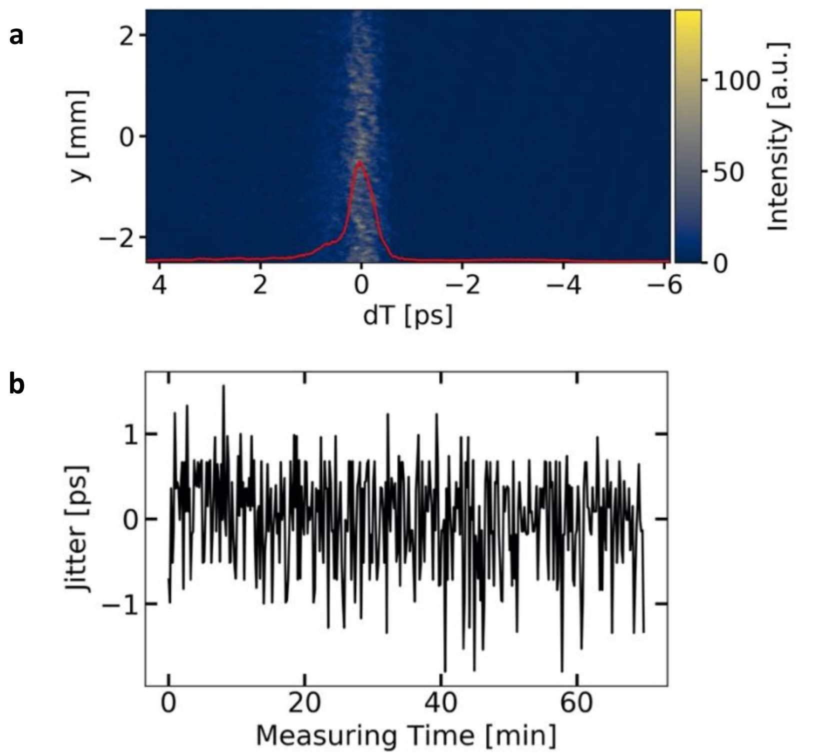

Supplementary Fig. 4 | Timing jitter between the electron beam and the probe pulse. a, A typical signal of the spatial-decoding taken by a CCD camera. The horizontal axis corresponds to the difference in the arrival time on the ZnTe between the electron beam and the probe pulse. **b**, Arrival time difference, i.e., timing jitter, consecutively obtained for ~1 h (391 shots in total). The RMS of the timing jitter was 0.43 ps.

4. Experimental setup 1: Echelon-based single-shot measurement to measure the electric field contraction with a high temporal resolution

In Supplementary Sections 4,5, we let the electron beam perpendicularly pass through the 1 mm thick ZnTe crystal (110), inducing a transverse electric field inside the crystal. Probe pulses (a part of the Ti:sapphire laser which is used for the generation of the electron beams) with a central wavelength of 800 nm and a pulse duration of ≤130 fs (FWHM) irradiated the ZnTe in the same direction as the electron beam path. The linear polarization of the probe pulses was parallel to the [-110] axis of the ZnTe to maximize the Pockels effect.

An echelon-based single-shot measurement[52,53] was conducted to obtain the spatiotemporal profile of the electric field around a relativistic electron beam with a high resolution. Supplementary Figs. 5a, b show the experimental setup. An echelon mirror, which has a step-like mirror surface, was used to convert the temporal information of the THz electric field into the spatial profile of the probe laser. Here, the probe pulse was reflected from the echelon mirror with a step width of 15 μm, step height of 3 μm, and step number of 1,000. The steps resulted in the temporal retardation (20 fs) among the beamlets reflected at each step. After the reflection, the probe pulses were focused by a cylindrical lens and injected into the ZnTe with a shape of a narrow line; the spatial profile was obtained along the line, and the temporal profile was measured on the line. The temporal information of the electric field inscribed on the probe pulse was extracted when the laser beam diverged after passing through the ZnTe. Cylindrical lenses downstream of the ZnTe were used for horizontal and vertical imaging of the probe pulse via a CCD camera. We applied the phase offset method to evaluate the electric field strength quantitatively with a high signal-to-noise ratio. Here, the setup was the same as the crossed-Nicol configuration except that a quarter-wave plate (QWP) with a slight offset rotation was positioned in front of the downstream polarizer. The relation between the measured probe intensity I and the retardation Γ, or relative phase shift of the probe pulse induced by the Pockels effect, is given by

$$\frac{I(\phi,\Gamma)}{I(\phi,0)} - \frac{I(-\phi,\Gamma)}{I(-\phi,0)} = \frac{2\sin\Gamma}{\sin\phi}, \quad (3)$$

where ϕ is the phase offset angle of the QWP. Here, $I(\phi, 0)$ corresponds to the background data recorded without an electron beam. The retardation and the THz electric field induced inside the EO crystal are related by

$$\Gamma = \frac{2\pi n_{PL}^3 d}{\lambda} r_{41} E_{THz}, \quad (4)$$

where n_{PL} is the refractive index of the EO crystal for the 800 nm probe laser, r_{41} is an EO constant, E_{THz} is the induced electric field strength, d is the thickness of the crystal, and λ is the wavelength of the probe laser. The concrete parameters are as follows: $n_{PL} = 2.85$, $r_{41} = 3.5$ pm/V, $d = 1.0$ mm, and $\lambda = 800$ nm. The value of the EO constant is experimentally acquired by adding a known electric field to the ZnTe crystal, which is 13 % smaller than the literature value of 4.0 pm/V (see ref.[32]). The electric field strength was obtained by measurement of the retardation.

Supplementary Figs. 6a–c show the raw data (CCD camera images) of the echelon-based single-shot measurement. To conduct the phase offset method and obtain the electric field strength in Fig. 2a, we used the signals obtained with the phase offset of $\phi = +1.5°$ and $\phi = -1.5°$ (Supplementary Figs. 6b, c) as $I(\phi, \Gamma)$ and $I(-\phi, \Gamma)$ in Eq. (3).

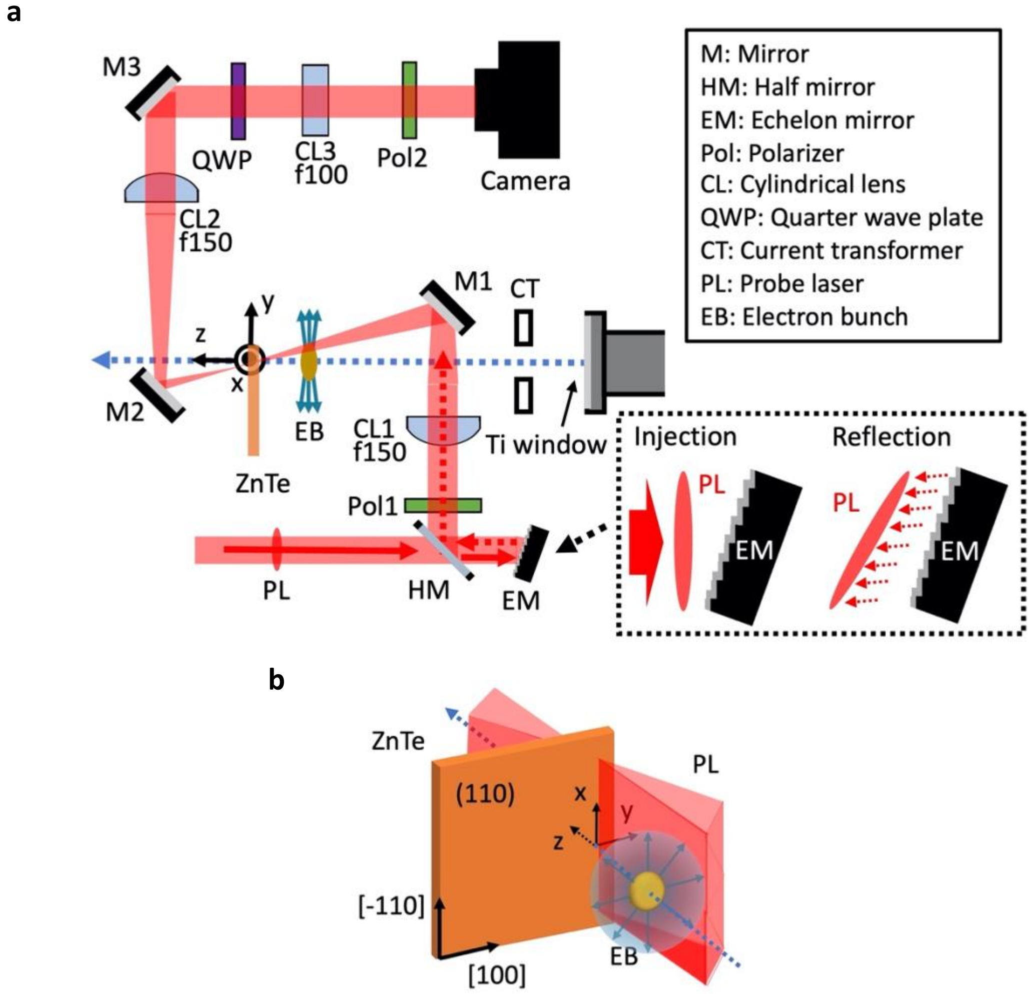

Supplementary Fig. 5 | Experimental setup of echelon-based single-shot measurement. a, A 2D schematic of the experimental setup. Abbreviations describing the setup are listed in the upper-right corner. Time delay is spatially imprinted on the probe laser by an echelon mirror; this imprinting converts a probe pulse to beamlets. Notably, each delay corresponds to the double length of the step height of the echelon mirror, as shown in the magnified images around the mirror in the black dashed rectangle. Red solid and dashed arrows denote the path of the probe laser before and after the reflection, respectively. The CL1 focuses the parallel beamlets into a line in the x-direction on the ZnTe, and the CL2 makes them parallel again. The distance between the CL1 and the echelon mirror is its focal length to suppress the divergence due to the step-like mirror surface. The CL3 is rotated 90° with respect to the CL1 and CL2 for imaging in the y-direction. Here, the magnifications in the x- and y-directions are 2.8 and 1.0 on the CCD camera, respectively. The relative angle between the Pol1 and Pol2 is 90°. We used the phase offset method by rotating the QWP. The incidence angle of the probe laser into the ZnTe was 25°, whereas the electron beam path was perpendicular. **b**, A 3D schematic around the ZnTe crystal before the electron beam hits the crystal. The PL is linearly focused on the crystal by the cylindrical lens. The polarization of the PL and the measured electric field are directed in the x-direction, which corresponds to the [-110] crystal axis.

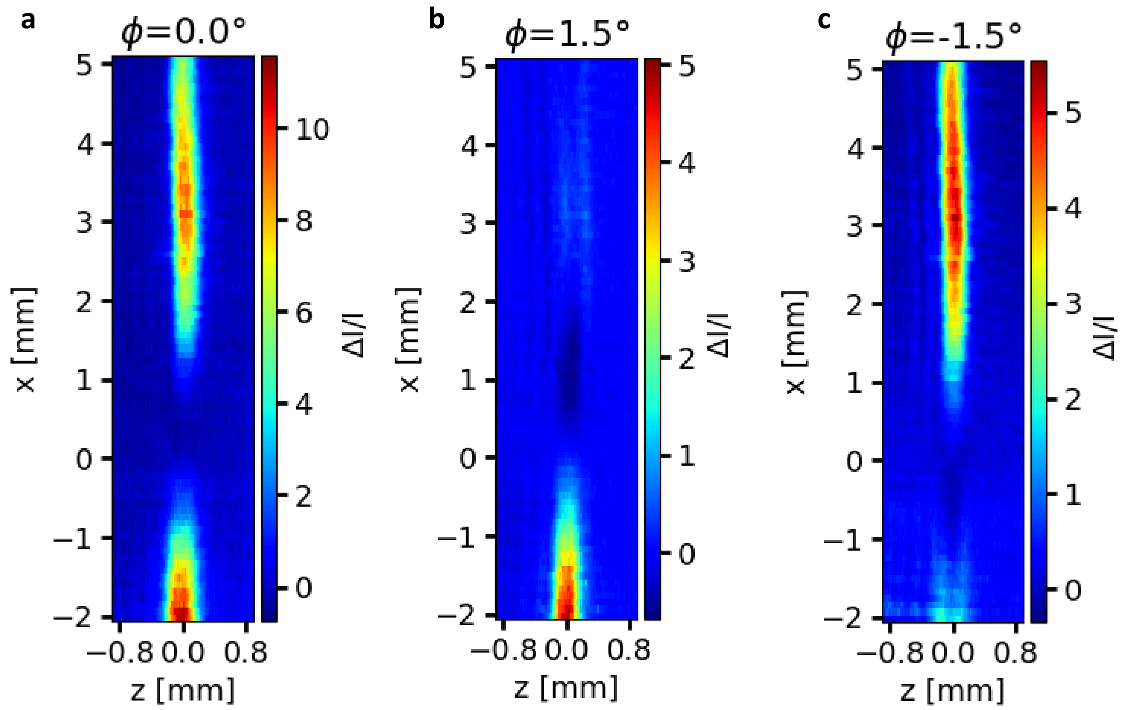

Supplementary Fig. 6 | Results of the echelon-based single-shot measurement. a–c, Spatiotemporal profiles of the electric field around a relativistic electron beam obtained through echelon-based single-shot measurement with phase offset $\phi = 0°$, $+1.5°$, and $-1.5°$. The color bar denotes the EO signal: $\Delta I/I = (I(\phi,\Gamma) - I(\phi,0))/I(\phi,0)$. Here **a** corresponds to the crossed-Nicol configuration. Fig. 2b shows the difference in the signal between **b** and **c**, i.e., the electric field profile obtained by the phase offset method.

5. Experimental setup 2: Balanced detection method to obtain the spherical electric field wavefront because of the transmission of a metallic boundary

Balanced detection was conducted using two photodiodes[54] to obtain the large spatiotemporal profile of the electric field for the spherical wavefront evolution. Supplementary Figs. 7a,b show the experimental setup. Here, the probe laser, whose polarity was modulated by the ZnTe, was divided into two pulses (i.e., pulses with *p*- and *s*-polarizations) by a polarized beam splitter (PBS). The two polarization components were then measured by two different photodiodes. The retardation Γ was obtained by the difference between the measured intensity of the *p*- and *s*-polarizations (I_p and I_s) according to the relation

$$\frac{I_p - I_s}{I_p + I_s} = \sin\Gamma\,. \tag{5}$$

Here, the THz electric field was also obtained by Eq. (4), as conducted in the phase offset method (Supplementary Section 4). The temporal profile was surveyed by the delay stage, where the time increment of the delay scan was 0.2 ps. The spatial profile was acquired by shifting the ZnTe crystal and all the optics around it in the direction perpendicular to the electron beam axis using a motorized stage with a step size of 1 mm (see Figs. 7a,b).

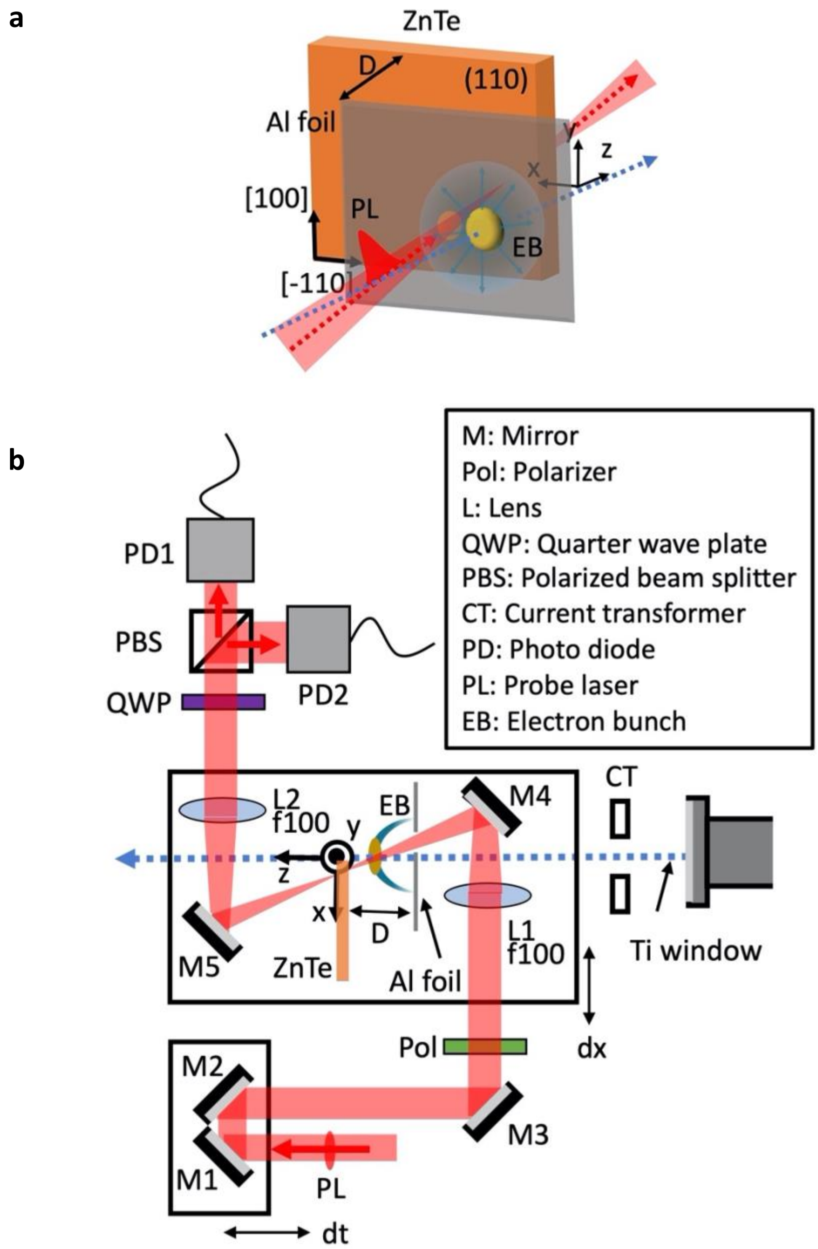

Supplementary Fig. 7 | Experimental setup used to measure the spatiotemporal evolution of the spherical electromagnetic wavefront. a, A 3D schematic around the ZnTe crystal. The focused probe pulse passed through the hole with the diameter of 1 mm in the Al foil and was incident on the crystal with an incidence angle of 37° while the electron beam passed through the Al foil. **b**, A 2D schematic of the experimental setup. Abbreviations describing the setup are listed in the upper-right corner. The probe laser was focused on the ZnTe crystal by a lens, and the transverse electric field on the spot was measured. The polarization of the probe pulse was directed along the x-axis, and the QWP was adjusted to divide the probe pulse into two (p- and s-polarization) pulses with the same intensities. The spatiotemporal profile of the electric field was measured by moving two motorized stages for shifting the optics around the ZnTe crystal and the delay stage, respectively; they are surrounded by black rectangles in the figure, and the two-way arrows show the moving direction (dx and dt). The position of the Al foil was moved in the z-direction, and the distance D was adjusted.

6. Comparisons between the experimental result and the theoretical calculation of the electric field contraction under the Lorentz transformation

The electric field strength profile and the pulse broadening obtained by the experiment and the theoretical calculation (see Supplementary Section 2), which corresponds to Figs. 2a,b, are shown in Supplementary Figs. 8a, b. To compensate the loss caused by the Fresnel reflection, the electric field strength of the experimental results is divided by the transmission coefficient in the field amplitude for a THz pulse perpendicularly injected into an interface between two materials with different refractive indexes:

$$t = \frac{2n_1}{n_1 + n_2} = 0.48\,, \qquad (6)$$

where n_1 and n_2 are the refractive indexes of the air and the ZnTe crystal in the THz range (n_1 =1.0 and n_2 =3.2), respectively.

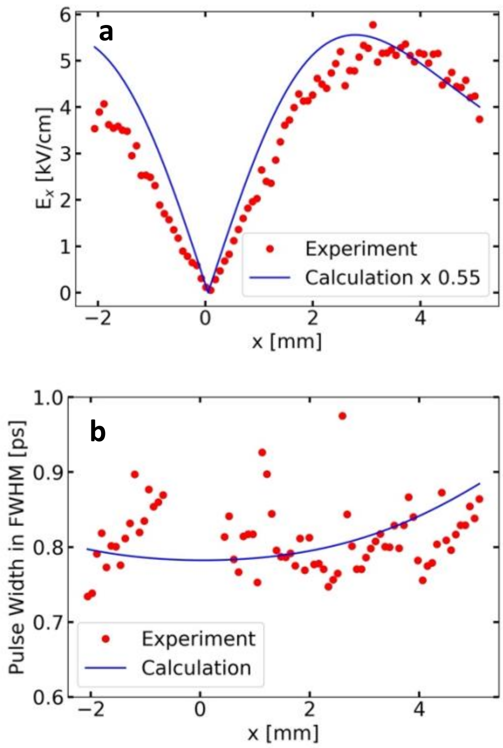

Supplementary Fig. 8 | Comparison of the electric field strength and the pulse broadening between the experiment and the calculation. a, Transverse electric field strength (E_x) of the experiment and calculation in the radial direction (x-axis). **b**, Pulse-width broadening in the radial direction. Red solid circles and blue curves denote the result of the experiment and the calculation given by the convolution between the beam profile in three dimensions and the transverse electric field around a relativistic electron, respectively. Some experimental data points around the beam axis in the pulse broadening result are excluded because of the worse signal-to-noise ratio. Notably, the pulse width of the THz electric field (~ 0.79 ps) at $x = 0$ mm is larger than the counterpart of the longitudinal beam size (~ 0.72 ps) in this energy region (35 MeV), as shown in **b**.

The electric field strength obtained in the experiment is about two times smaller than that of the calculation. There are some possibilities which cause the underestimation of the experimental values and overestimation of the calculated values of the electric field. The calculations were performed in vacuum, but we performed the experiment in the air. The effect of vapor absorption for THz pulses should be considered; roughly 10 % loss of the peak amplitude is expected. The other effects such as the absorption of the THz pulse inside the ZnTe, the frequency-dependent phase mismatch between the THz pulse and the probe laser inside the ZnTe, and the dispersive propagation of the THz pulse inside the ZnTe should be considered. This discrepancy will be investigated in future work.

7. Comparisons of the electric field strength and the pulse broadening between the experimental result and the simulation of the spherical electric field wavefront

The electric field strength profile and the pulse broadening obtained by the experiment and the simulation (see Methods), which corresponds to Figs. 3a–d, are shown in Supplementary Figs.

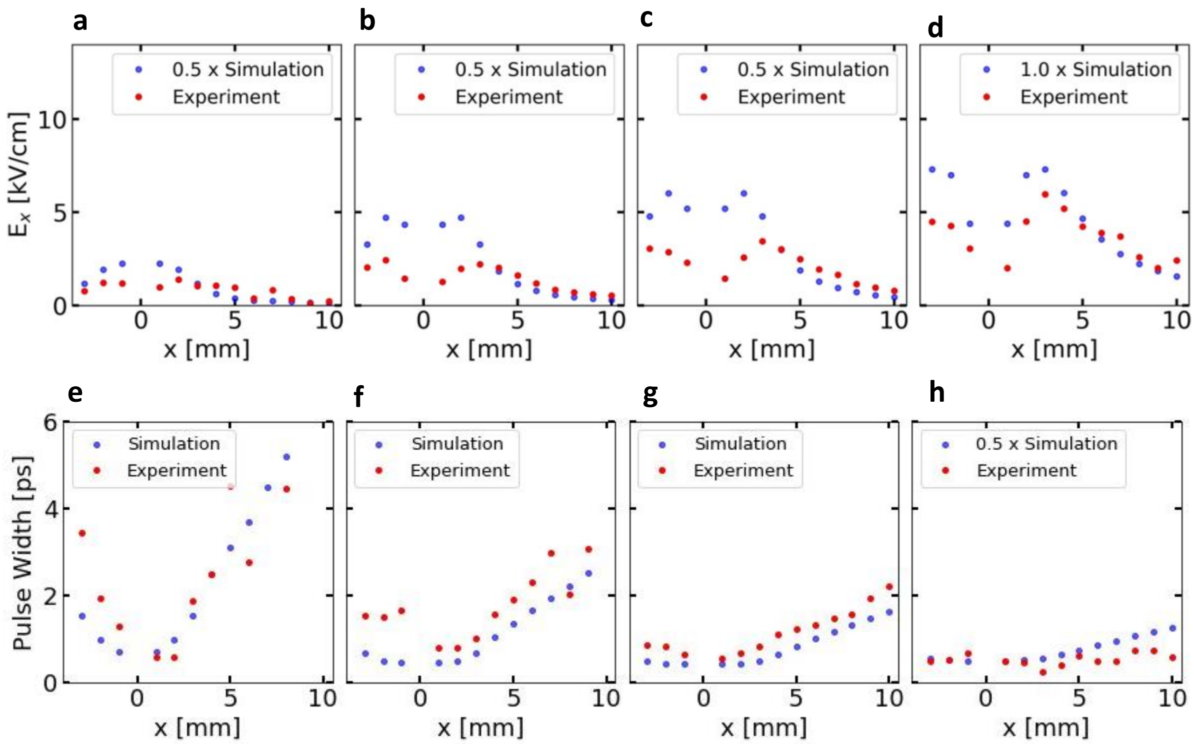

Supplementary Fig. 9 | Comparing the strength profile and the pulse broadening of the electric field in the radial direction around the electron beam, as obtained from the experiment and the simulation. a–**h**, The electric field strength profile (**a**–**d**) and pulse broadening (**e**–**h**) in the radial direction for the propagation distances of 5, 15, 25, and 209 $(= D)$ mm after the cancellation of the electric field. Blue and red solid circles denote the simulation and experimental results, respectively. The results in **a**–**c** and **e**–**g** show a good coincidence between the results of the experiment and those of the PIC simulation. The difference of the electric field strength between the experiment and the simulation in **a**–**c** is confirmed (see Section 6). However, the tendency observed in **d** differs from the other subfigures (i.e., **a**–**c**): the compensation factor changes from 0.5 to 1.0. In addition to that, the compensation factor is introduced in **h**. This difference arises mainly because the results **d** and **h** are obtained in a cylindrical coordinate instead of the 3D coordinate and also because of the numerical Cherenkov radiation caused by the long propagation distance, or long simulation time.

9a–d and Supplementary Figs. 9e–h, respectively. In addition to the Fresnel reflection discussed in Section 6, we have included the effect of the oblique incidence of the probe laser. We considered the difference between the polarization of the probe laser and the [-100] axis of the ZnTe. The electric field strength is multiplied by a compensation factor of 0.98 derived by the cosine of 10.8° corresponding the refracting angle of the probe laser in the ZnTe crystal, where the incidence angle is 37° on the crystal surface. On the other hand, the compensation factor is 1.0 in Section 6 because the probe laser has the s-polarization.

8. Two-dimensional snapshots of the electric field profile derived by the simulation

The experimental results obtained by EO sampling is the spatiotemporal profile of the electric field. This is different from the snapshot of the profile in 2D space. This is the reason why the theoretical wavefront function shown in Figs. 3e–h is not a sphere but a parabolic shape, i.e.,

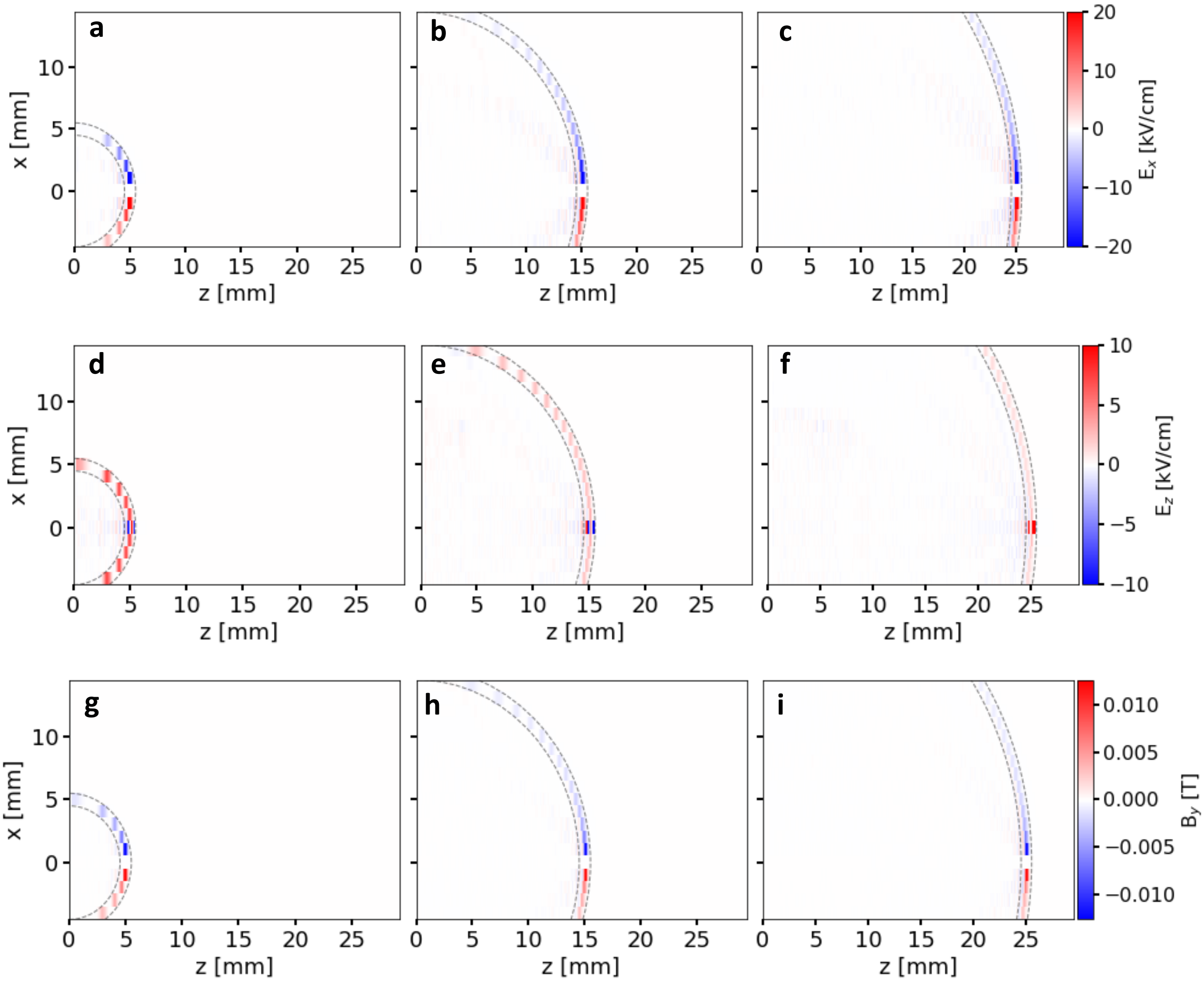

Supplementary Fig. 10 | Snapshots of the electromagnetic field around a relativistic electron beam with an infinitesimal diameter acquired by the PIC simulation. a–i, 2D transverse (**a**–**c**) and longitudinal (**d**–**f**) electric fields (E_x, E_z), and a magnetic field circulating around the beam axis ($x = y = 0$) (**g**–**i**) (B_y) in the xz-plane at the time when an electron beam with an infinitesimal diameter, a pulse width of 1.0 ps (FWHM), an energy of 35 MeV, and a charge amount of 70 pC propagates for 5, 15, and 25 ($= D$) mm after the metallic boundary ($z = 0$ mm), as obtained by the PIC simulation. The black dashed lines are part of a sphere with a radius of $D - 0.5$ and $D + 0.5$ mm.

$z' = -\sqrt{x^2 + D^2} + 2D$. Supplementary Figs. 10a–i show the 2D snapshots of the electromagnetic wavefronts around the electron beam with an infinitesimal diameter propagates for distances (D) of 5, 15, and 25 mm given by the particle-in-cell simulation. These results show that the spherical wavefront is a perfect sphere with a radius identical to the propagation distance and with the center at the position on the metallic boundary where the electron beam passes through.

Reference

48. Nozawa, I. *et al.* Measurement of <20fs bunch length using coherent transition radiation. *Phys. Rev. Spec. Top. - Accel. Beams* **17**, 72803 (2014).
49. Shan, J. *et al.* Single-shot measurement of terahertz electromagnetic pulses by use of electro-optic sampling. *Opt. Lett.* **25**, 426 (2000).
50. Wilke, I. *et al.* Single-Shot Electron-Beam Bunch Length Measurements. *Phys. Rev. Lett.* **88**, 124801 (2002).
51. Berden, G. *et al.* Electro-optic technique with improved time resolution for real-time, nondestructive, single-shot measurements of femtosecond electron bunch profiles. *Phys. Rev. Lett.* **93**, 114802 (2004).
52. Poulin, P. R. & Nelson, K. A. Irreversible Organic Crystalline Chemistry Monitored in Real Time. *Science* **313**, 1756–1760 (2006).
53. Asai, G. *et al.* High-throughput terahertz spectral line imaging using an echelon mirror. *Opt. Express* **29**, 3515–3523 (2021).
54. Ota, M. *et al.* Longitudinal and transverse spatial beam profile measurement of relativistic electron bunch by electro-optic sampling. *Appl. Phys. Express* **14**, 26503 (2021).